Journal of Dispersion Science and Technology
Publication details, including instructions for authors and subscription information:
http://www.tandfonline.com/loi/ldis20

Effects of Reaction Sequence on the Colloidal Polypyrrole Nanostructures and Conductivity

Juyoung Choi [a], Hyungtae Kim [a], Seungjoo Haam [a] & Sang-Yup Lee [a]
[a] Department of Chemical and Biomolecular Engineering, Yonsei University, Seoul, Korea
Version of record first published: 13 May 2010.

To cite this article: Juyoung Choi, Hyungtae Kim, Seungjoo Haam & Sang-Yup Lee (2010): Effects of Reaction Sequence on the Colloidal Polypyrrole Nanostructures and Conductivity, Journal of Dispersion Science and Technology, 31:6, 743-749

To link to this article: http://dx.doi.org/10.1080/01932690903332954

Journal of Dispersion Science and Technology, 31:743–749, 2010

ISSN: 0193-2691 print/1532-2351 online
DOI: 10.1080/01932690903332954

Taylor & Francis
Taylor & Francis Group

Effects of Reaction Sequence on the Colloidal Polypyrrole Nanostructures and Conductivity

Juyoung Choi, Hyungtae Kim, Seungjoo Haam, and Sang-Yup Lee

Department of Chemical and Biomolecular Engineering, Yonsei University, Seoul, Korea

The relationship between nanoscaled morphology and macroscopic electrical conductivity of polypyrrole (PPy) nanostructures was qualitatively investigated. The PPy nanostructures were prepared via microemulsion polymerization using ionic surfactants. The morphology of PPy was influenced by both the type of ionic surfactants and reaction sequences; specifically, the PPy structures were highly influenced by the reaction sequence when anionic surfactant of SDS was used. By changing reaction sequence, a gel-like PPy was formed influencing on the macroscopic electrical conductivity. The results indicate that the macroscopic conductivity of PPy is affected by its nanoscaled structures as determined by the reaction conditions.

Keywords Conductivity, ionic surfactant, nanostructure, polypyrrole

1. INTRODUCTION

Polypyrrole (PPy), a conducting polymer, has been widely studied because of its various applications in electrical devices such as batteries and sensors.[1–4] For these promising applications, a variety of fabrication methods of PPy in the form of films,[5–7] nanoparticles,[8–11] and nanotubes[12,13] have been developed. In general, the PPy nanoparticles and nanotubes were prepared via oxidative polymerization of pyrrole (Py) monomer requiring soft template such as microemulsion. Because the structure of soft template can be modified by controlling the physicochemical reaction parameters such as surfactant concentration and temperature, the soft template-based oxidative PPy polymerization is a promising method to control the morphologies and physical properties of PPy.[14,15]

Surfactant and dopant molecules are the key factors determining morphology and electrical conductivity of PPy product prepared via microemulsion technique. The electrical conductivity of PPy is influenced by the existence of dopant molecule that associates with Py backbone. The anionic surfactant can work as a dopant molecule by associating with the positive PPy. Thereby, the effects of anionic surfactant in preparation of PPy are so complex specifically when it is used as a templating molecule. This dopant role of surfactant highly influences on the conductivity of PPy product.[14] However, the morphology in nanoscale can change the overall conductivity, too. Thus, it is required to make an inspection on the relation between nanoscaled morphology and macroscopic physical property.

In this report, the morphology and surface property of PPy nanostructures prepared from different types of surfactants and reaction sequences were investigated with the consideration of the electrical conductivity. The morphologies of the product were changed by both the types of surfactant used and addition sequence of reactants. This morphology change was closely related to the surface coverage of surfactant and influenced on the electrical conductivity.

2. MATERIALS AND METHODS

2.1. Chemicals

Pyrrole monomer (98%), ammonium persulfate ($(NH_4)_2O_8S_2$, 98%), sodium dodecyl sulfate (SDS, 99%), and tetradecyl trimethyl ammonium bromide (TTAB, 99%) were purchased from Aldrich (St. Louis, MO, USA) and used as received without further purification.

2.2. Polypyrrole Nanostructure Synthesis

Polypyrrole nanostructures were synthesized in an aqueous solution containing surfactants. In general, Py monomer was dropped into surfactant solution with a vigorous stirring to construct microemulsion, and then oxidant solution was added to initiate polymerization. Herein, the PPy nanostructure samples were labeled in the form of "surfactant name-PPy." For example, when the PPy nanostructure was prepared using SDS, it was labeled as SDS-PPy. When the addition sequences of oxidant and pyrrole monomer was reversed (i.e., surfactant, oxidant,

Received 6 January 2009; accepted 1 February 2009.

This work was supported by Korea Science and Engineering Foundation (Grant number: KOSEF 2007-8-1158).

Address correspondence to Sang-Yup Lee, Department of Chemical and Biomolecular Engineering, Yonsei University, Seoul 120-749, Korea. E-mail: leessy@yonsei.ac.kr

and pyrrole monomer were added in sequence), the products were presented as "R-surfactant name-PPy" in the text.

In preparing PPy samples, a general preparation procedure is given in the reference.[9] Details of our experiments are given as follows; the cationic surfactant-based PPy nanostructures were synthesized using tetradecyl trimethyl ammonium bromide (TTAB). First, 2.02 g of TTAB (6×10^{-3} mol) was dissolved in 30 ml of distilled water and stirred at room temperature for 1 hour. A volume of 0.2 ml pyrrole monomer dropped into the surfactant solution slowly with stirring. The pyrrole solution was stirred for another 6 hours to form microemulsion. To this microemulsion solution, 5.8 ml of $(NH_4)_2O_8S_2$ aqueous solution (0.5 M) was slowly added. The color of micelle solution turned into black after adding oxidant. The polymerization continued for 12 hours. The synthesized polypyrrole nanostructures were completely washed 3 times with ethanol following centrifugation in order to remove any remaining chemicals. Exactly same experimental sequences were followed for SDS-based PPy preparation. As described ahead, the addition sequences of oxidant and pyrrole monomer were reversed, when preparing R-TTAB-PPy and R-SDS-PPy samples. In all experiments the surfactant concentration is higher than the critical micelle concentration of each surfactant (15.6 mM for TTAB and 8.1 mM for SDS, respectively.[16,17]).

2.3. Characterization

Morphologies of synthesized PPy nanostructures were observed using transmission electron microscopy (TEM, LIBRA 120, 100KeV). In preparing TEM samples, the PPy nanostructure solution was diluted with ethanol, and then positioned on the carbon-coated copper gird. Additional stain was not applied to prevent artifacts.

Sizes of synthesized PPy nanostructures were also investigated using a commercial dynamic light scattering (DLS) system (Photal Otsuka Electronics, ELS-Z, Japan). To observe the hydrodynamic diameter variation during the reaction, 5 µl of PPy sample was taken at every an hour and dispersed in 1.5 ml water. This dilution is required to give sufficient signal intensity of the sample otherwise any reliable signal cannot be obtained. The hydrodynamic sizes were measured five times per each sample, and then the average and standard deviation of sizes were calculated. The particle size distribution was simultaneously obtained from the measurement. In order to investigate the surface charge and surfactant coverage of PPy nanostructures, zeta potential measurement was carried out using a commercial laser-Doppler zeta potential meter (Nano ZS 3000, Malvern Instruments, USA). In the zeta potential measurement, the PPy nanostructures were suspended in 1 mM KCl solution at different pH. The concentration of 1 mM was chosen as a reference concentration in order to fix the Debye screening length used in calculation of surface charge density. More than five times of measurements were carried out for each sample and the average and standard deviation were obtained.

For the chemical analysis and electrical conductivity measurement, PPy powder was prepared by drying in a vacuum oven at 60°C over 8 hours. The chemical analysis was performed using a FTIR spectroscopy (FT/IR-460 Plus, JASCO, USA). FTIR analysis in transmittance mode was performed after making the PPy powder to pellet by compressing with KBr powder. The conductivities of PPy nanostructures were examined using 4-point probe (IM6e, Zahner, Germany) after preparing PPy pellet in a diameter of 13 mm and 0.3 mm thickness.

3. RESULTS AND DISCUSSION

First, the morphologies of PPy nanostructures were investigated. In Figure 1, TEM images of PPy nanostructures prepared by different types of ionic surfactant and preparation sequences were present. When the cationic surfactant of TTAB was used as a capping molecule, well-dispersed spherical PPy nanoparticles were obtained (Figure 1a) though some aggregates were also found. These particles had smooth surfaces in average diameter of 55.8 nm. On the other hand, only the aggregated structures of PPy nanoparticles were observed when anionic surfactant of SDS was used (Figure 1b). This aggregated structure made porous assembly of nanoparticles similar to the previous PPy studies.[9,18] The average diameter of SDS-PPy nanoparticles was 23.1 nm. Considering the electrical charges of the surfactant used, one potential factor to aggregate the SDS-PPy is the interaction between SDS and positively charged PPy, which could destabilize the PPy nanoparticles.

By changing the addition sequence of the reactant, drastic morphology changes were induced. When the oxidant of ammonium peroxydisulfate was dissolved in the micelle solution before adding PPy monomer, the PPy monomer reacts in the suspending medium and its diffusion into the micelle was limited. Thus, irregular gel-like structures were generated due to the polymerization in the medium. In the R-TTAB-PPy sample, any spherical structure of PPy was not found. Only irregularly shaped PPy nanostructures were found (Figure 1c). Formation of irregular structure of PPy is because TTAB micelle formation was interrupted. Chelation takes place between tetradecyl trimethyl ammonium cation in TTAB and anionic sulfonate groups in ammonium persulfate preventing micelle formation.[19] The chelated TTAB molecules aggregated to settle down forming a white precipitation instead of making a stable emulsion. On the other hand, mixed structures of nanospheres and random gel-like structures were made in the R-SDS-PPy (Figure 1d). This mixed

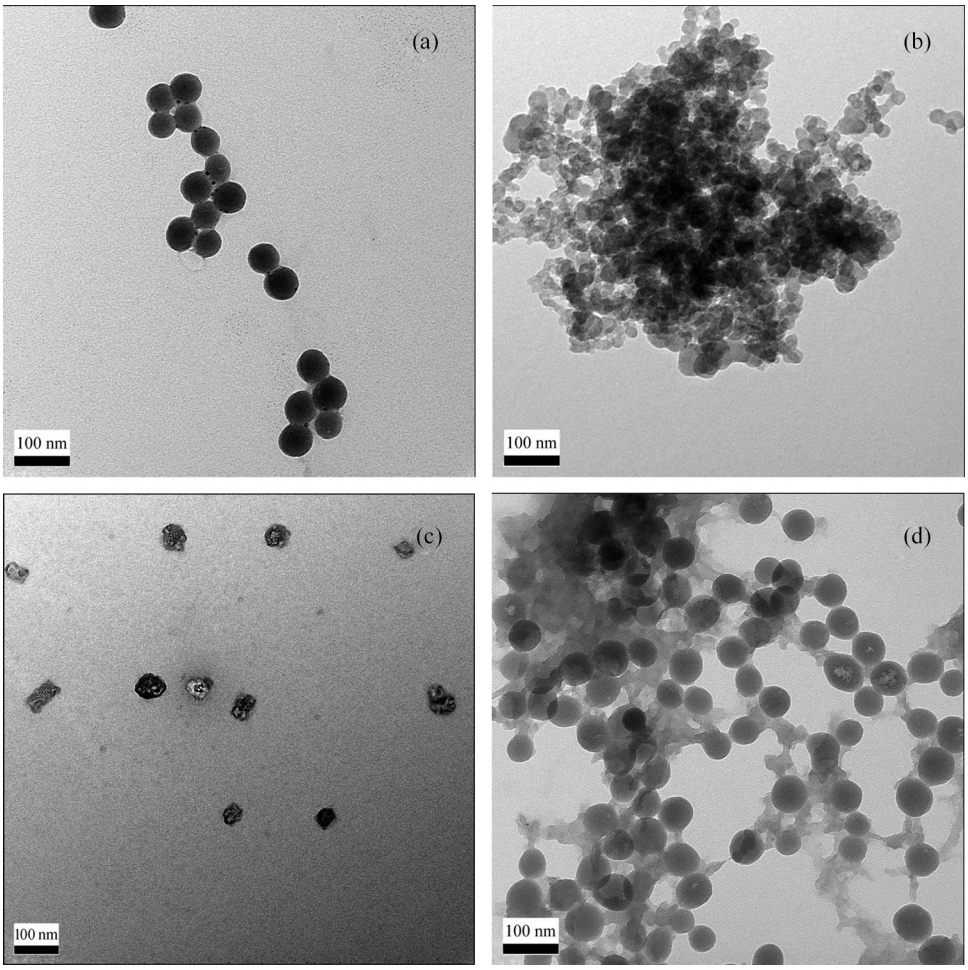

FIG. 1. TEM images of PPy nanostructures. (a) TTAB-PPy, (b) SDS-PPy, (c) R-TTAB-PPy, (d) R-SDS-PPy.

morphology suggests that polymerization of pyrrole monomer are taking place both in the micelle and bulk solution. The average diameter of sphere in R-SDS sample was 55.8 nm which is similar to the diameter of TTAB-PPy. Because both oxidant and SDS would have same negative charge, the micelle formation was not disturbed in R-SDS-PPy sample. The amorphous gel-like structure was likely to be made in the continuous phase by the reaction of monomers initiated by the ammonium peroxydisulfate dissolved in the continuous phase. These observations indicate that the morphology of PPy nanostructure can be controlled by changing the addition sequence of reactants.

To support PPy nanostructure changes by the reaction sequence, the hydrodynamic diameter and size distribution were monitored using dynamic light scattering (DLS) system. The hydrodynamic diameter changes provide information on the development of PPy nanostructures during the reaction. In Figure 2a, the average hydrodynamic diameter changes of each SDS-based sample are present. The hydrodynamic diameters of the product PPy nanostructures were about 1.5 times larger than the sizes observed in the TEM images. This discrepancy of the size is due to the aggregates of PPy.

There was a difference in hydrodynamic diameter growth with the reaction sequence. The size of SDS-PPy would grow slowly until around 4 hours while the size of R-SDS-PPy would hardly change after 1 hour. The continuous size increase of SDS-PPy suggests that the PPy nanostructures continuously aggregate with each other. This size growth mechanism is also supported by the size distribution changes. The particle size distribution is present in Figure 2b. For the SDS-PPy sample, the size distribution is getting broad with time due to the aggregation of PPy nanostructures. However, the size distribution of R-SDS-PPy was changed little after 1 hour of reaction. This little change indicates that the PPy nanostructures are made at the early stage of reaction. These hydrodynamic diameter and size distribution changes suggests that the nanostructures of SDS-PPy continuously aggregate and the nanostructures of the R-SDS-PPy were

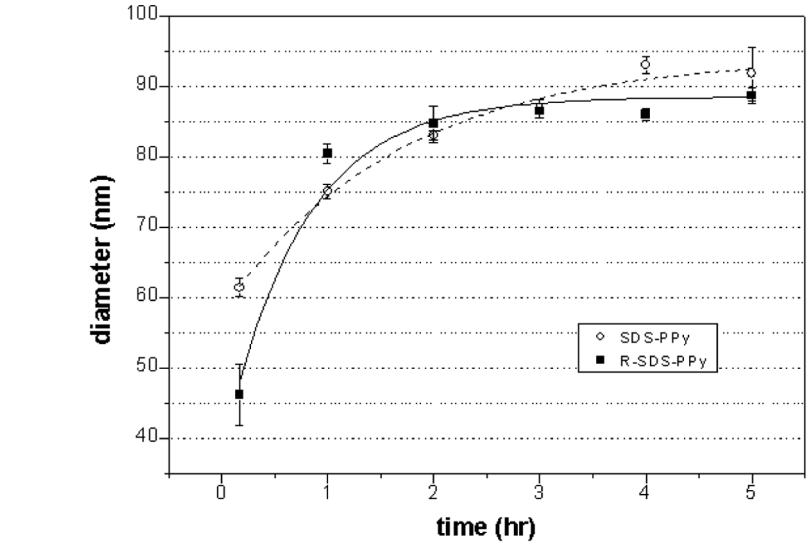

(a)

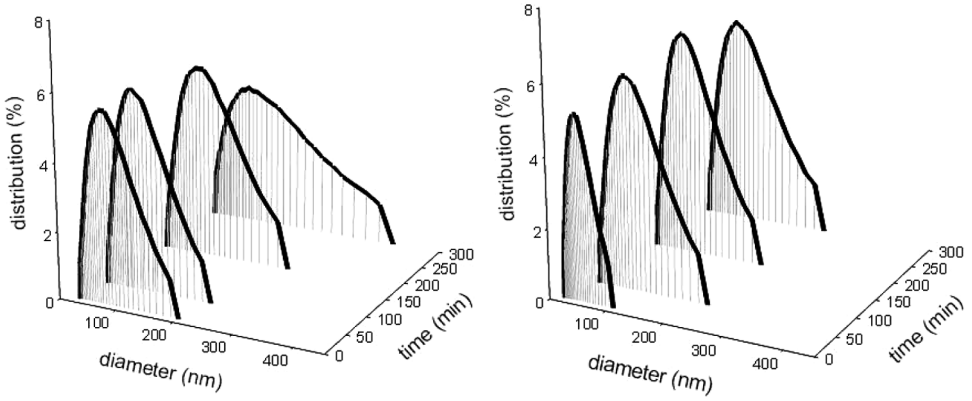

(b)

FIG. 2. (a) Hydrodynamic diameter changes of SDS-PPy (white circle) and R-SDS-PPy (black square); (b) size distribution changes of SDS-PPy (left) and R-SDS-PPy (right).

formed at the early stage of reaction and remained constant.

Because the PPy nanostructures were influenced by the surfactant type and addition sequences, the surfactant coverage should also be investigated. To inspect the surfactant coverage, the surface charge density of PPy nanostructures was calculated and then the relative surface coverage was estimated. To determine the surface charge density, the zeta potential of PPy nanostructures was measured. In zeta potential measurement, all PPy samples were assumed as spherical particles though aggregates are not exactly spherical. In Figure 3, changes of zeta potential values were plotted against the solution pH. The TTAB-PPy sample had isoelectric point (pI) of 11.0, higher than the pI of surfactant-free PPy, 10.0,[20] while the SDS-PPy showed pI of 8.5 ~ 9.0. The high pI value of TTAB-PPy samples is likely due to the coverage of positively charged trimethyl ammonium cation on the TTAB-PPy surface as well as the surface-exposed PPy itself. In addition, the PPy nanoparticle had overall positive zeta potential values under 25 mV even when anionic surfactant of SDS was used. This value of zeta potential suggests incomplete coverage of SDS on the PPy nanostructure considering that PPy has positive surface charge with a zeta potential of 40 mV.[20,21] Interestingly, the positive zeta potential values of R-SDS-PPy were slightly higher than those of SDS-PPy sample. This higher value of zeta potential is likely due to the contribution from the amorphous gel-like region which is positively charged by the adsorption of proton.[20]

From the zeta potential data, the surface charge density of PPy nanostructure was calculated. The PPy nanostructures were assumed as monodisperse spherical particles whose radius was estimated from TEM images. The surface charge density was obtained using an analytical solution

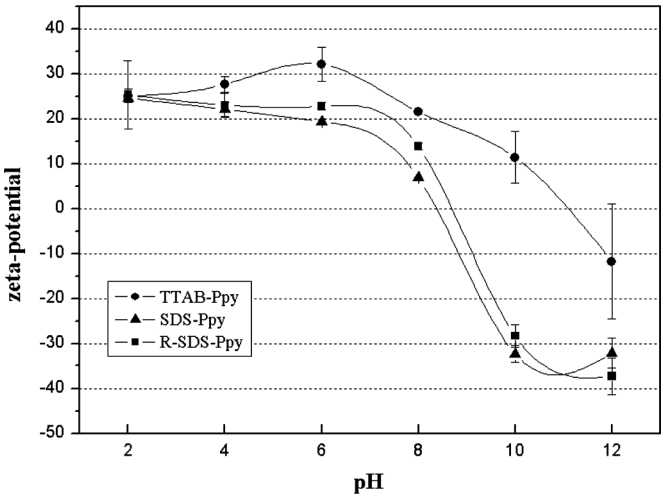

FIG. 3. Zeta potential of PPy nanostructures (lines are provided as a guide).

developed by Ohshima et al. where surface potential and Debye screening length were used as parameters in calculation.[22] Equation (1) is used in calculation of the surface charge density.

$$\sigma = \frac{\varepsilon_0 \varepsilon_r \kappa k T}{e} \cdot 2\sinh\left(\frac{y_s}{2}\right) \times \left[1 + \frac{2}{A\cosh^2(y_s/4)} + \frac{8\ln[\cosh(y_s/4)]}{A^2\sinh^2(y_s/2)}\right]^{1/2} \quad \cdots\cdots \quad [1]$$

$$\text{where } \kappa = \left(\frac{2ne^2}{\varepsilon_0 \varepsilon_r kT}\right) A = \kappa a, \text{ and } y_s = \frac{e\zeta}{kT}$$

In Equation (1), e is the elementary electric charge, n is the electrolyte concentration, ε_0 is vacuum permittivity, ε_0 is dielectric constant of suspending medium, and ζ is zeta potential of the PPy samples. In calculation, the measured zeta potential values were used instead of surface potential, so that the calculation results would indicate the surface charge density at the shear plane. The Debey screening length (κ^{-1}) is set as 9.64 nm at 25°C for 1 mM monovalent ionic solution.

To minimize the proton and hydroxide adsorption on the surface, the surface charge densities at pH 6.0 were compared. The calculated surface charged density is summarized in Table 1. The surface charge density of TTAB-PPy agreed with that of surfactant-free PPy.[20] This surface charge density agreement and spherical morphology indicate that the TTAB-PPy nanostructure is capped with TTAB. However, the surface charge reduced notably when the SDS was used. This reduction of surface charge density is originated from the existence of negative charge of the anionic head group in SDS molecule. R-SDS-PPy had higher surface charge density than SDS-PPy. This charge density increment of R-SDS-PPy is probably due to the contribution from surfactant-free PPy that forms an amorphous gel in TEM images. Assuming that TTAB covers entire surface of PPy nanostructure, the coverage of SDS molecules in the SDS-based PPy nanostructures could be estimated. It was turned out that SDS covers only 42% and 32% of surfaces for SDS-PPy and R-SDS–PPy, respectively.

TABLE 1
The surface charge density and relative surface coverage of each polypyrrole sample

	TTAB-PPy	SDS-PPy	R-SDS-PPy
Surface charge density (mC/m^2)	3.314	1.947	2.254
Relative surfactant coverage (%)	(100%)	41.4%	31.8%

The chemical composition of PPy nanostructures were inspected through the FTIR spectroscopy. FTIR spectra of each PPy sample are present in Figure 4. For the TTAB-PPy, the characteristic peak of ammonium persulfate coupled with Py is clearly indicated at 1187 cm^{-1} corresponding to S=O stretching of sulfonate.[14] Another peak at 1109 cm^{-1} represents weakened sulfate bond after association of Py with ammonium persulfate.[18] The methyl chain of TTAB is observed at 2848 and 2917 cm^{-1}.[23] With this methyl peak of TTAB, it is notable that the peak position at 924 cm^{-1} agrees with that of surfactant-free PPy. This agreement suggests that the TTAB would not chemically associate with PPy nanostructure. All the other peaks of TTAB-based sample were matched well with PPy prepared without any surfactant (surfactant-free PPy).

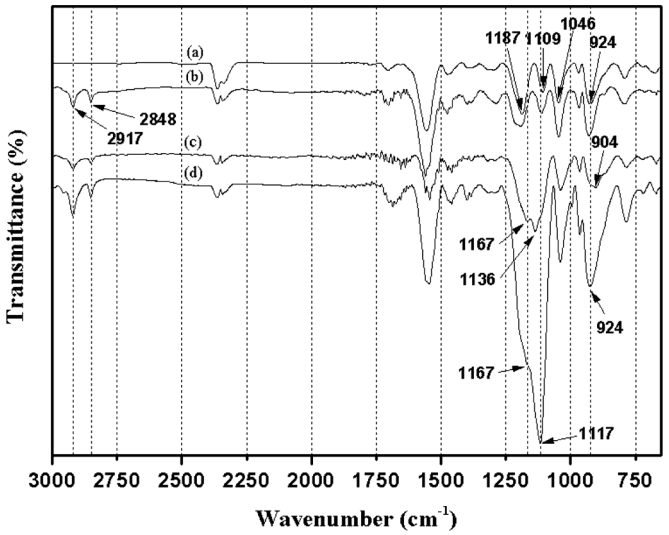

FIG. 4. Infrared spectra of surfactant-free PPy (a), TTAB-PPy (b), SDS-PPy (c), and R-SDS–PPy (d).

The infrared (IR) spectra of SDS-based PPy nanostructures showed strong characteristic peaks at 1167 cm^{-1} corresponding to the S=O symmetric stretching vibration of sulfonate and at 1136 cm^{-1} of sulfate.[24] The highly increased peak of these SO_3^- and SO_4^{2-} indicates the association of SDS with Py. From these strong peak signals, it is inferred that many SDS molecules were in the SDS-PPy nanostructure. On the other hand, sulfate peak at 1136 cm^{-1} was shifted to 1117 cm^{-1} in R-SDS-PPy. This peak is locating between sulfate peak positions of surfactant free-PPy and SDS-PPy because of the overlapping of them. This overlapping also supports coexistence of both SDS-covered and surfactant-free PPy nanostructures. In addition, the existence of surfactant-free PPy in R-SDS-PPy was proved by the matching of C-H deformation peaks at 924 cm^{-1}. This peak was commonly observed in surfactant-free PPy, TTAB-PPy, and R-SDS-PPy. Considering the C-H deformation peak is locating at 904 cm^{-1} in SDS-PPy, the peak at 924 cm^{-1} indicates the existence of surfactant-free PPy.

Finally, the effects of nanostructures on the macroscopic electrical conductivities were examined. The measured conductivities of each PPy nanostructures were present in Figure 5. The conductivity of PPy prepared without addition of surfactant was tested as a reference experiment. The conductivity of surfactant-free PPy was very low (3.78×10^{-3} S/cm, left bar) when only ammonium persulfate was used. This value is similar to those of previous reports.[10,25] Conductivity of TTAB-PPy nanostructures was in the same order with surfactant-free PPy. However, conductivity of SDS-PPy was highly increased because of the association of SDS to PPy working as a dopant molecule. In contrast, the R-SDS-PPy showed low conductivity similar to that of surfactant-free PPy. This low conductivity is due to the inhibition of electrical conduction by the amorphous surfactant-free PPy. The amorphous gel-like PPy would have low conductivity like the surfactant-free PPy. Thus, it behaves as an electrical resistor. When the R-SDS-PPy nanostructures were made into a pellet, these amorphous regions would behave as electrical resistors resulting in low conductivity. These measurements clearly indicate that the structural changes of PPy in nanoscale would influence on the bulk property of electrical conductivity. The conductivity of PPy nanostructures agrees with the FTIR peak intensity ratio of 1560 cm^{-1} against 1475 cm^{-1} present in Table 2. These two peaks represent C=C and C-C stretching of PPy, respectively, and higher ratio represents longer effective π-conjugation along the PPy chains.[26] These results support that the molecular structures of PPy products were influenced by the change of reaction sequence.

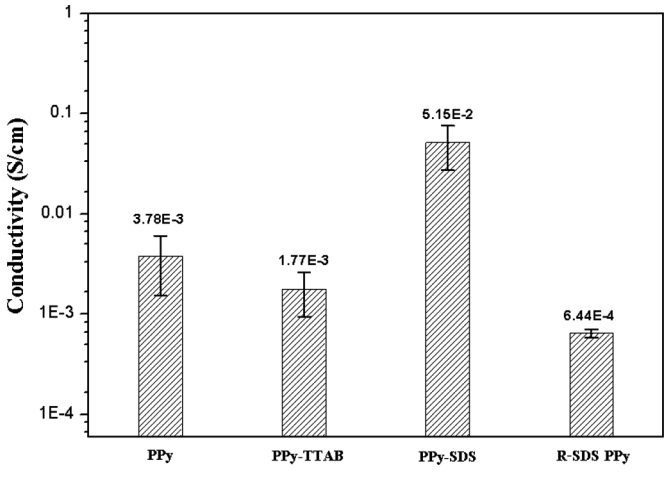

FIG. 5. Comparison of the electrical conductivities of each polypyrrole nanostructure.

TABLE 2
Peak intensity ratio of each polypyrrole nanostructure

	Surfactant-free PPy	SDS-PPy	R-SDS-PPy
Intensity ratio (C=C/C-C)	0.891	0.978	0.912

4. SUMMARY

The morphology and electrical conductivity of PPy nanostructures were influenced by both the type of ionic surfactant and the addition sequence of the reactants. The morphologies of PPy nanostructures were changed by the surfactant type that associates with Py monomer. The addition sequence of reactant drastically changed the nanostructure morphology, size distribution, surface coverage of surfactant, and electrical conductivity. In addition, the electrical conductivity was reduced by the existence of amorphous PPy in the nanostructure which plays as a resistor. These outcomes could be applied in conducting polymer fabrication as well as microemulsion-based nanoparticle synthesis study.

REFERENCES

[1] Jang, J. (2006) *Adv. Polym. Sci.*, 199: 189–259.
[2] Wang, J., Too, C.O., and Wallace, G.G. (2005) *J. Power Sources*, 150: 223–228.
[3] Yoon, H., Chang, M., and Jang, J. (2006) *J. Phys. Chem. B*, 110: 14074–14077.
[4] Ko, S. and Jang, J. (2007) *Biomacromolecules*, 8: 182–187.
[5] Wu, A., Kolla, H., and Manohar, S.K. (2005) *Macromolecules*, 38: 7873–7875.
[6] Liu, Y.C. (2002) *Langmuir*, 18: 174–181.

[7] Lisboa, P., Gilliand, D., Ceccone, G., Valsesia, A., and Rossi, F. (2006) *Appl. Surf. Sci.*, 252: 4397–4401.
[8] Simmons, M.R., Chaloner, P.A., and Armes, S.P. (1998) *Langmuir*, 14: 611–618.
[9] Wang, H., Lin, T., and Kaynak, A. (2005) *Synth. Met.*, 151: 136–140.
[10] Liu, Y., Chu, Y., and Yang, L. (2006) *Mater. Chem. Phys.*, 98: 304–308.
[11] Cairns, D.B. and Armes, S.P. (1999) *Langmuir*, 15: 8052–8058.
[12] Jang, J. and Oh, J.H. (2002) *Chem. Comm.*, 2200–2201.
[13] Xiao, R., Cho, S.I., Liu, R., and Lee, S.B. (2007) *J. Am. Chem. Soc.*, 129: 4483–4489.
[14] Omastová, M., Trchová, M., Kovárová, J., and Stejskal, J. (2003) *Synth. Met.*, 138: 447–455.
[15] Zhang, X., Zhang, J., Song, W., and Liu, Z. (2006) *J. Phys. Chem. B*, 110: 1158–1165.
[16] Garcia-Mateos, I., Velázuez, M.M., and Rodriguez, L.J. (1990) *Langmuir*, 6: 1078–1083.
[17] Cifuentes, A., Bernal, J.L., and Diez-Masa, J.C. (1997) *Langmuir*, 9: 4271–4274.
[18] Omastová, M., Trchová, M., Pionteck, J., Prokeš, J., and Stejskal, J. (2004) *Synth. Met.*, 143: 153–161.
[19] Son, A.J.R., Lee, H., and Moon, B. (2007) *Synth. Met.*, 157: 597–602.
[20] Zhang, X. and Bai, R. (2003) *Langmuir*, 19: 10703–10709.
[21] Jang, J., Nam, Y., and Yoon, H. (2005) *Adv. Mater.*, 17: 1382–1386.
[22] Ohshima, H., Healy, T.W., and White, L.R. (1982) *J. Coll. Interface Sci.*, 90: 17–26.
[23] Krishnakumar, V. and Seshadri, S. (2007) *Spectrochim. Acta A*, 68: 833–838.
[24] Prissanaroon, W., Ruangchuay, L., Sirivat, A., and Schwank, J. (2000) *Synth. Met.*, 114: 65–72.
[25] Ayad, M.M. (1994) *J. Appl. Polym. Sci.*, 53: 1331–1337.
[26] Yan, F., Xue, G., and Zhou, M.J. (2000) *Appl. Polym. Sci.*, 77: 135–140.